Heliyon 10 (2024) e32498

Contents lists available at ScienceDirect

Heliyon

journal homepage: www.cell.com/heliyon

Research article

CircFgfr2 promotes osteogenic differentiation of rat dental follicle cells by targeting the miR-133a-3p/DLX3 signaling pathway

Cheng Xu [a,b,1], Zhiqing Xu [a,1], Guixian Li [c], Jing Li [d], Li Ye [a], Yang Ning [a,*], Yu Du [a,**]

[a] Hospital of Stomatology, Guangdong Provincial Key Laboratory of Stomatology, Guanghua School of Stomatology, Sun Yat-sen University, Guangzhou, Guangdong, China
[b] Nanjing Stomatological Hospital, Affiliated Hospital of Medical School, Reasearch Institute of Stomatology, Nanjing University,Nanjing, Jiangsu, China
[c] Operative Dentistry and Endodontics, Jiangmen Municipal Stomatological Hospital, Jiangmen, Guangdong, China
[d] Department of Stomatology, Shenzhen Hospital, Southern Medical University, Shenzhen, Guangdong, China

ARTICLE INFO

Keywords:
CircFgfr2
Dental follicle cells
Osteogenesis differentiation

ABSTRACT

Dental follicle cells (DFCs) promote bone regeneration *in vivo* and *in vitro*. Circular RNAs (circRNAs) play crucial roles in bone development and regeneration. Our previous study demonstrated the upregulation of circFgfr2 expression during the osteogenic differentiation of DFCs. However, the molecular mechanisms and functional roles of circFgfr2 in DFCs osteogenesis remain unclear. In this study, we aimed to investigate the subcellular localization of circFgfr2 in DFCs using fluorescence *in situ* hybridization. *In vitro* investigations demonstrated that circFgfr2 overexpression promoted osteogenic differentiation, as evidenced by real-time quantitative polymerase chain reaction. By integrating the outcomes of bioinformatics analyses, dual luciferase reporter experiments, and chromatin isolation by RNA purification, we identified circFgfr2 as a sponge for miR-133a-3p, a key regulator of osteogenic differentiation. Moreover, miR-133a-3p suppressed osteogenic differentiation by targeting DLX3 and RUNX2 in DFCs. We validated that circFgfr2 promoted the osteogenic differentiation of DFCs through the miR-133a-3p/DLX3 axis. To further investigate the therapeutic potential of circFgfr2 in bone regeneration, we conducted *in vivo* experiments and histological analyses. Overall, these results confirmed the crucial role of circFgfr2 in promoting osteogenesis. In summary, our findings demonstrated that the circFgfr2/miR-133a-3p/DLX3 pathway acts as a cascade, thereby identifying circFgfr2 as a promising molecular target for bone tissue engineering.

1. Introduction

Periodontitis is a chronic, progressive inflammatory condition characterized by the loss of periodontal attachment and resorption of the alveolar bone, leading to clinical symptoms such as tooth loosening and potential tooth loss [1]. Regeneration of lost alveolar bone presents a significant treatment challenge [2]. Currently, guided bone tissue regeneration technology is used for alveolar bone reconstruction in clinical practice. However, its clinical efficacy is inconsistent, and its applicability is limited [3]. In recent years,

* Corresponding author.
** Corresponding author.
E-mail addresses: ningyang@mail.sysu.edu.cn (Y. Ning), duyu3@mail.sysu.edu.cn (Y. Du).
[1] Cheng Xu and Zhiqing Xu contributed equally to this study.

https://doi.org/10.1016/j.heliyon.2024.e32498
Received 12 February 2024; Received in revised form 4 June 2024; Accepted 5 June 2024
Available online 6 June 2024
2405-8440/© 2024 Published by Elsevier Ltd. This is an open access article under the CC BY-NC-ND license (http://creativecommons.org/licenses/by-nc-nd/4.0/).

research focus has shifted toward the regeneration of alveolar bone using stem cells, with dental follicle cells (DFCs) identified as promising seed cells capable of osteogenesis and differentiation within an inflammatory environment [4]. However, the molecular mechanism underlying the osteogenic differentiation of DFCs remains unclear. As research progresses, the role of circular RNAs (circRNAs) in the osteogenic differentiation of DFCs has garnered increasing attention.

CircRNAs constitute a distinct class of endogenous non-coding RNAs formed by pre-mRNA back-splicing. CircRNAs, featuring a closed-loop structure devoid of free 3′ and 5′ ends, exhibit resistance to RNase R digestion and demonstrate tissue-specific expression predominantly in the cytoplasm [5,6]. Emerging evidence indicates that circRNAs play essential roles in embryonic development and cell activities such as cell growth and osteogenesis [7,8]. High-throughput sequencing technologies and bioinformatics have facilitated the identification of numerous critical circRNAs involved in tissue regeneration processes [9], and they have also been found to participate in osteogenesis [10,11]. During the osteogenic differentiation of dental pulp stem cells (DPSCs), 65 upregulated and 22 downregulated circRNAs have been identified [12]. Another study indicated that circRNA124534 was overexpressed during osteogenic differentiation, and that the overexpression of circRNA124534 in human periodontal ligament stem cells (hPDLSCs) induced osteogenesis *in vitro* and *in vivo* [7]. In our previous study, we reported 138 upregulated and 128 downregulated circRNAs during the osteogenic differentiation of rat DFCs, potentially involving the mitogen-activated protein kinases (MAPK) and transforming growth factor-β (TGF-β) signaling pathways [13].

CircRNAs may regulate the synthesis of parental genes, proteins, and short peptides [10,11,14]. Moreover, circRNAs can serve as competing endogenous miRNA sponges to modulate target genes [15,16]. Several studies have shown that circRNA expression regulates osteogenic differentiation by sponging miRNAs. For example, circ0026827 promotes osteogenic differentiation in DPSCs by acting as a sponge for miR-188-3p and regulating the Beclin1 and RUNX1 signaling pathways [7]. CircFKBP5 serves as an osteogenic regulator in DPSCs by sponging miR-708-5p and targeting GIT2 [17]. The circRNAs BANP and ITCH interact with miR-34a and miR-146a, promoting osteogenic differentiation in PDLSCs through the MAPK pathway [18]. CircRNA CDR1as promotes the osteogenic differentiation of PDLSCs by inhibiting miR-7 [16]. However, few studies have investigated the mechanisms of action of circRNAs in DFCs.

In our previous study, we discovered that circFgfr2 is significantly upregulated during osteogenic induction in DFCs and during postnatal dental follicle development, indicating that circFgfr2 plays a key role in the osteogenic differentiation of DFCs [13]. Additionally, we demonstrated that the overexpression of circFgfr2 in DFCs results in decreased miR-133 expression [13]. However, the molecular mechanisms and functional roles of circFgfr2 in DFC osteogenesis remain unclear. In this study, we aimed to investigate the functional roles and underlying mechanisms of action of circFgfr2 in DFCs during osteogenesis. By revealing the novel mechanisms of osteogenic differentiation of DFCs, our findings may guide the future development of therapeutic strategies for bone-defect regeneration.

2. Materials and methods

2.1. Culture and identification of DFCs

Sprague-Dawley rats (postnatal 5–7 days) were obtained from the Laboratory Animal Center, Sun Yat - sen University for our study. Rats were euthanized with pentobarbital sodium and immersed in 75 % ethanol for 10 min. Dental follicles were carefully isolated from the tooth germs of the first and second mandibular molars of each rat and cultured in α-modified Eagle's medium (Gibco, USA) supplemented with 20 % fetal bovine serum (FBS) (Gibco, USA) and 1 % penicillin/streptomycin (Gibco, USA). The DFCs were incubated at 37 °C under 5 % CO2. The medium was changed every 3 days until the cells reached approximately 80 % confluence. Flow cytometry (FCM) was performed using anti-CD29, CD34, CD44, CD45, and CD90 antibodies (1:200, Abcam, UK) to identify the DFCs.

2.2. Sanger sequencing and Agarose gel electrophoresis

Specific divergent primers were designed based on the circRNA circularization site. Sanger sequencing was performed on the amplified products using these divergent primers. Total RNA from DFCs was extracted using Trizol reagent, and cDNA was synthesized through reverse transcription using arbitrary primers, with or without treatment with RNase R. Next, cDNA was amplified using convergent and divergent primers. Agarose gel electrophoresis was conducted to visualize the PCR products.

2.3. Fluorescence in situ hybridization (FISH)

The probe labeled with CY3 was designed for the circFgfr2 sequence and used for *in situ* hybridization. The DFCs were fixed with 4 % paraformaldehyde for 5 min at 4 °C, treated with 0.5 % Triton X-100 for 15 min at room temperature, and incubated with 100 % alcohol for 1 min. The samples were then dehydrated and air dried. The probe was prepared, and the hybridization buffer with the probe was denatured at 88 °C for 5 min. After hybridization, the slides were washed with 2 × SSC for 5 min at 42 °C, followed by two washes with 2 × SSC at room temperature for 5 min each. Then, 50 μL of DAPI-Antifade solution was applied onto the slide, the slide was covered, and it was incubated at room temperature in the dark for 20 min. Finally, the slides were observed under a fluorescence microscope.

2.4. Cell transfection

The full-length cDNA of circFgfr2 was amplified from DFCs and cloned into the specific vector pLC5-ciR (Geneseed, China) between the *Bam*HI and *Eco*RI sites for over-expression of circFgfr2 (pLC5-ciR-circFgfr2). The mock plasmid pLC5-ciR (NC) without the circFgfr2 cDNA was used as a control. Immunofluorescence was performed for verification of transfection according to the manufacturer's instructions. To overexpress or inhibit miR-133a-3p, miR-133a-3p mimics, miR-133a-3p inhibitors and NC-mimics were purchased (ThermoFisher, USA). The DFCs were transfected with the aforementioned plasmids and mimics using Lipofectamine 3000 (Invitrogen, USA) according to the manufacturer's instructions. After 48 h, the DFCs were harvested and used for further research.

2.5. Real-time quantitative polymerase chain reaction (RT-qPCR)

Total RNA was extracted using Trizol reagent (Invitrogen, USA). The extracted total RNA was reverse transcribed into cDNA using the Geneseed® II First Strand cDNA Synthesis Kit (Geneseed, China). The qRT-PCR was performed to detect the relative mRNA and miRNA expression levels using the Geneseed® qPCR SYBR® Green Master Mix (Geneseed, China). GAPDH or U6 was used as an internal control. All reactions were performed in triplicates and the fold expression changes were calculated using the comparative 2–ΔΔCt method. The PCR primers (Forevergen, China) used in this study are listed in Table 1.

2.6. CircRNA analysis and target prediction

The genomic loci of the FGFR2 gene and circFgfr2 were analyzed using the NCBI database (https://www.ncbi.nlm.nih.gov/). Then the binding sites of miR-133a-3p and miR-133a-5p with circFgfr2 were predicted using RegRNA 2.0 (http://regrna2.mbc.nctu.edu.tw/). The downstream genes of the miRNAs were predicted using the miRDB (http://mirdb.org/index.html), Targetscan (http://www.targetscan.org/vert_71/), and microT-CDS (http://diana.imis.athena-innovation.gr/DianaTools/index.php?r=microT_CDS/index) databases.

2.7. Dual-luciferase reporter assay (DLR)

PsiCHECK2.0 dual luciferase reporter vectors, containing wild type (WT) circFgfr2 (circFgfr2 WT) and WT DLX3 3′UTR (DLX3 WT), as well as their respective mutant forms (circFgfr2 MUT 1, circFgfr2 MUT 2, circFgfr2 MUT 3, and DLX3 MUT), were constructed (Geneseed, China). To investigate if miR-133a-5p directly targets circFgfr2, 293T cells were co-transfected with circFgfr2 WT or circFgfr2 MUT 1, along with miR-133a-5p mimics or a negative control (NC). Similarly, to assess if miR-133a-3p directly targets circFgfr2, 293T cells were co-transfected with circFgfr2 WT or circFgfr2 MUT 2 and/or circFgfr2 MUT 3, along with miR-133a-3p mimics or NC. Additionally, in order to determine the interaction between miR-133a-3p and the DLX3 gene, another dual-luciferase reporter assay method was utilized. DLX3 WT or DLX3 MUT was co-transfected with miR-133a-3p mimics and NC mimics into 293T cells. After 48 h of co-transfection, luciferase activity was measured using the Dual-Glo@Luciferase Assay System E2940 (Promega, USA), following the manufacturer's instructions. Firefly luciferase activities were normalized to Renilla luminescence in each well. All experiments were repeated at least three times.

2.8. Chromatin isolation by RNA purification (ChIRP)

Biotin-labeled circFgfr2 antisense DNA probes were designed and synthesized (Geneseed, China). The probes had biotin labeling at the 3-prime end and their sequences were as follows: 1.GTGCTCCAACAACATCAAGG-Bio; 2.GTACGGTGCTCCAACAACAT-Bio. ChIRP analysis was carried out following the protocols outlined by Chu et al. [19]. As a control, LacZ probes were used as a non-specific probe. Total RNA was collected, and qRT-PCR was performed to verify the circFgfr2 probes and the interaction between circFgfr2 and miR-133a-3p and miR-133a-5p.

2.9. Alkaline phosphatase (ALP) activity assay

ALP activity was measured using AKP/ALP test kits (Nanjing Jiancheng, China), following the manufacturer's instructions. In brief,

Table 1
The primers used in this study.

Gene name	Forward (5′-3′)	Reverse (5′-3′)
circFgfr2	GTCCCATCAGACAAAGGCA	GCAGGGACAGCATGGAG
miR-133a-3p	CCTTTGGTCCCCTTCA	TGGTGTCGTGGAGTCG
miR-133a-5p	GCCGAGAGCTGGTAAAATGG	TGGTGTCGTGGAGTCG
RUNX2	AACCAAGTGGCCAGGTTCAA	GGATGAGGAATGCGCCCTAA
OPN	CAGTCGATGTCCCTGACGG	GTTGCTGTCCTGATCAGAGG
DLX3	GCCTCACACAAACACAGGTGA	GTGGTACCAGGAGTTGGTGG
GAPDH	TCCATGGCACCGTCAAG	CAGCCTTCTCCATGGTGG
U6	CTCGCTTCGGCAGCACA	AACGCTTCACGAATTTGCGT

cells were seeded in 96-well plates and cell lysates were collected. The samples were incubated at room temperature for 5–10 min and diluted with a buffer to a final volume of 100 μL in a 96-well plate. Subsequently, the fluorescence was measured at a wavelength of 405 nm. To visualize ALP staining, DFCs were fixed in 4 % paraformaldehyde for 10 min and then subjected to ALP staining using the ALP staining kit (Beyotime, China), as per the manufacturer's instructions.

2.10. Alizarin Red staining

DFCs were washed twice with PBS, fixed with 4 % paraformaldehyde for 10 min, and subsequently stained with Alizarin Red staining solution (Nanjing Jiancheng, China) at room temperature for 30 min.

2.11. In vivo implantation

Twelve 8-week-old BALB/c nude male mice were randomly divided into 3 groups (n = 4) based on the type of implanted scaffolds: β-TCP scaffolds (Dimension: 5 mm × 5 mm × 2 mm, Dingan Technology, China), $DFCs^{OE\text{-}circFgfr2}$/β-TCP scaffolds, and $DFCs^{NC\text{-}circFgfr2}$/β-TCP scaffolds. The OE-circFgfr2 and NC-circFgfr2 DFCs were seeded onto the β-TCP scaffold at a density of 1×10^6 cells. After anesthesia by peritoneal injection of 1.5 % pentobarbital sodium, a total of 8 scaffolds were implanted into the dorsal region of the mice. After 8 weeks, the animals were euthanized using an excessive dose of pentobarbital sodium.

2.12. Histological analysis

All samples were fixed, demineralized, dehydrated, and embedded in paraffin. Paraffin-embedded specimens were then sectioned at a thickness of 5 μm and stained with hematoxylin and eosin (HE) as well as Masson's trichrome. For immunohistochemistry staining, the sections were immersed in 3 % H_2O_2 after deparaffinization to eliminate the activity of endogenous peroxidase at 37 °C for 15 min and blocked with 5 % BSA in PBS for 1 h to exclude the non-specific binding. The sections were incubated with DLX3 antibody (1:100, Santa Cruz, USA), RUNX2 antibody (1:100, Santa Cruz, USA), COL1 antibody (1:100, Proteintech, USA) and OPN (1:100, Proteintech, USA).Then, the slides were incubated with appropriate secondary antibody at room temperature for 1 h. Finally, we detected the immunoactivity with an HRP-streptavidin detection system (GeneTech, China),and counterstained the slides with hematoxylin. Images of the stained sections were captured using a Leica Aperio AT2 microscope and analyzed using Aperio ImageScope software.

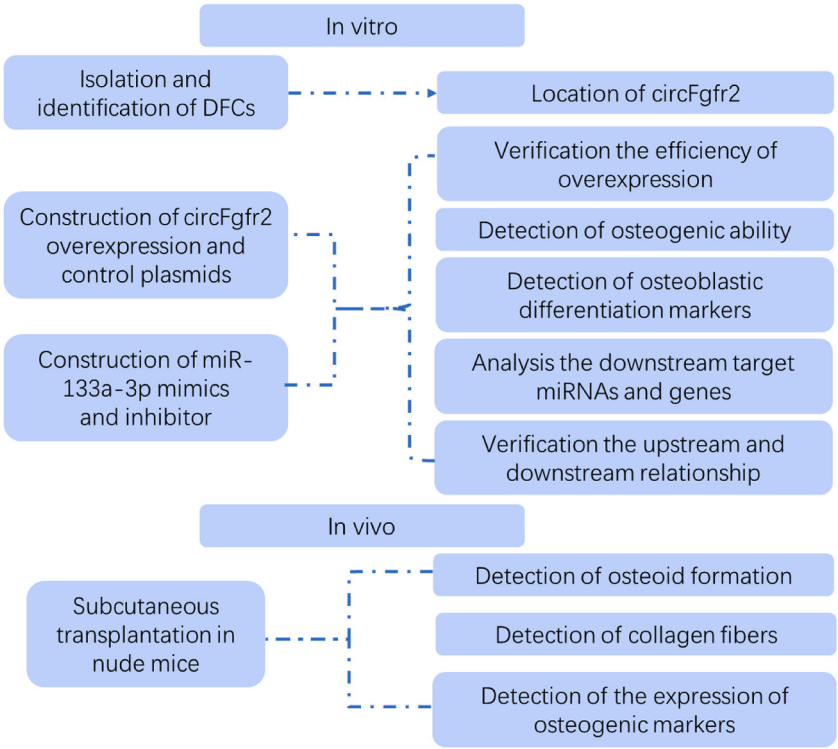

Fig. 1. Study workflow.

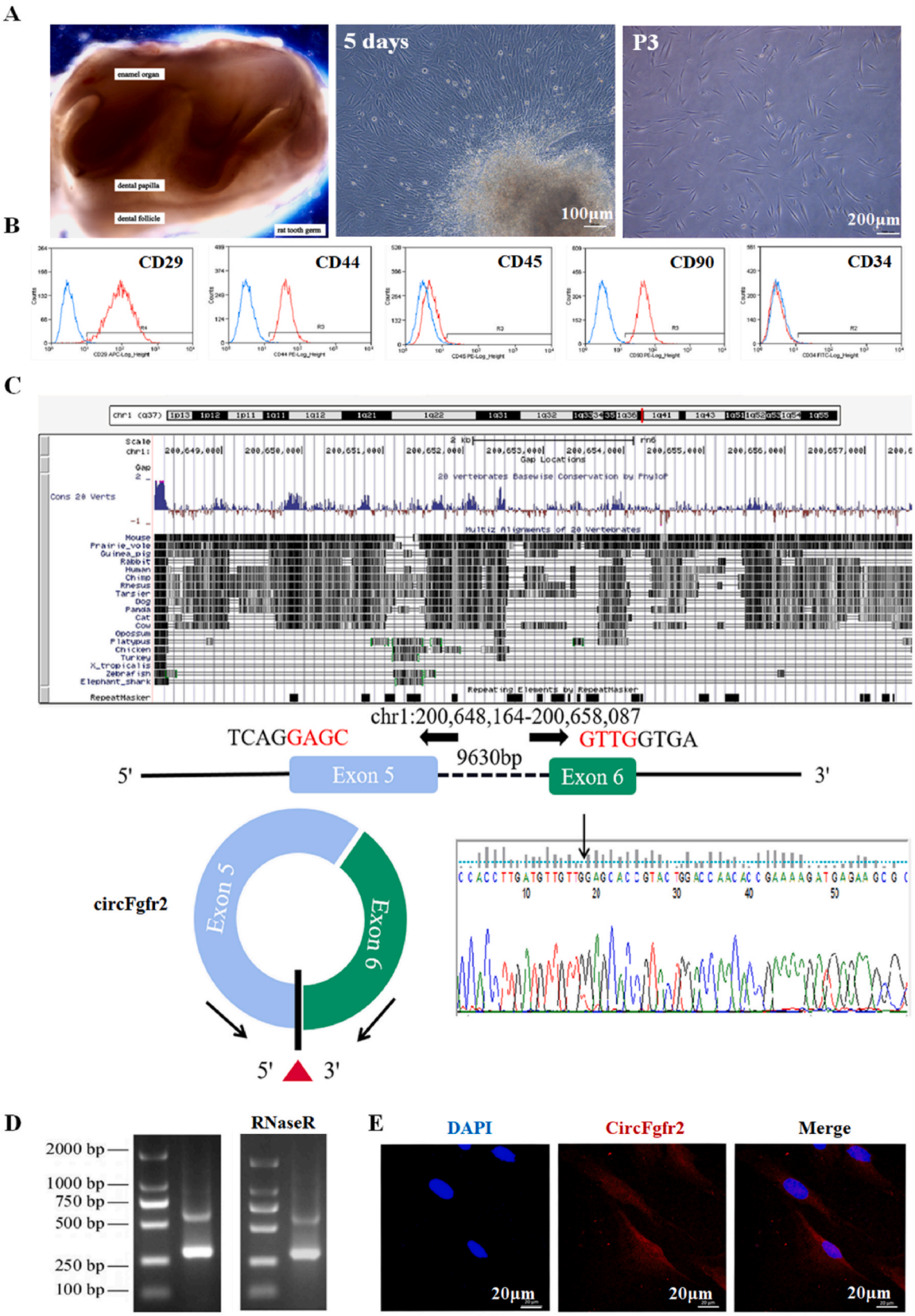

(caption on next page)

Fig. 2. Characterization of DFCs and circFgfr2 (A) Morphology of DFCs (× 20). Scale bar: 200 μm. (B) Representative FCM histograms indicating the expression levels of CD29, CD90, CD45, CD44, and CD34. (C) Sanger sequencing for the characterization and location of circFgfr2. (D) Agarose gel electrophoresis analysis indicating the expression of circFgfr2. (E) Fluorescence *in situ* hybridization showing the subcellular location of circFgfr2 in DFCs. Scale bar: 20 μm.

2.13. Statistical analysis

The results are expressed as mean ± standard deviation. Statistical significance was determined using unpaired *t*-test and one-way ANOVA. All data were analyzed using Prism 7.04 software (GraphPad Software, USA). A p-value less than 0.05 ($P < 0.05$) was considered statistically significant.

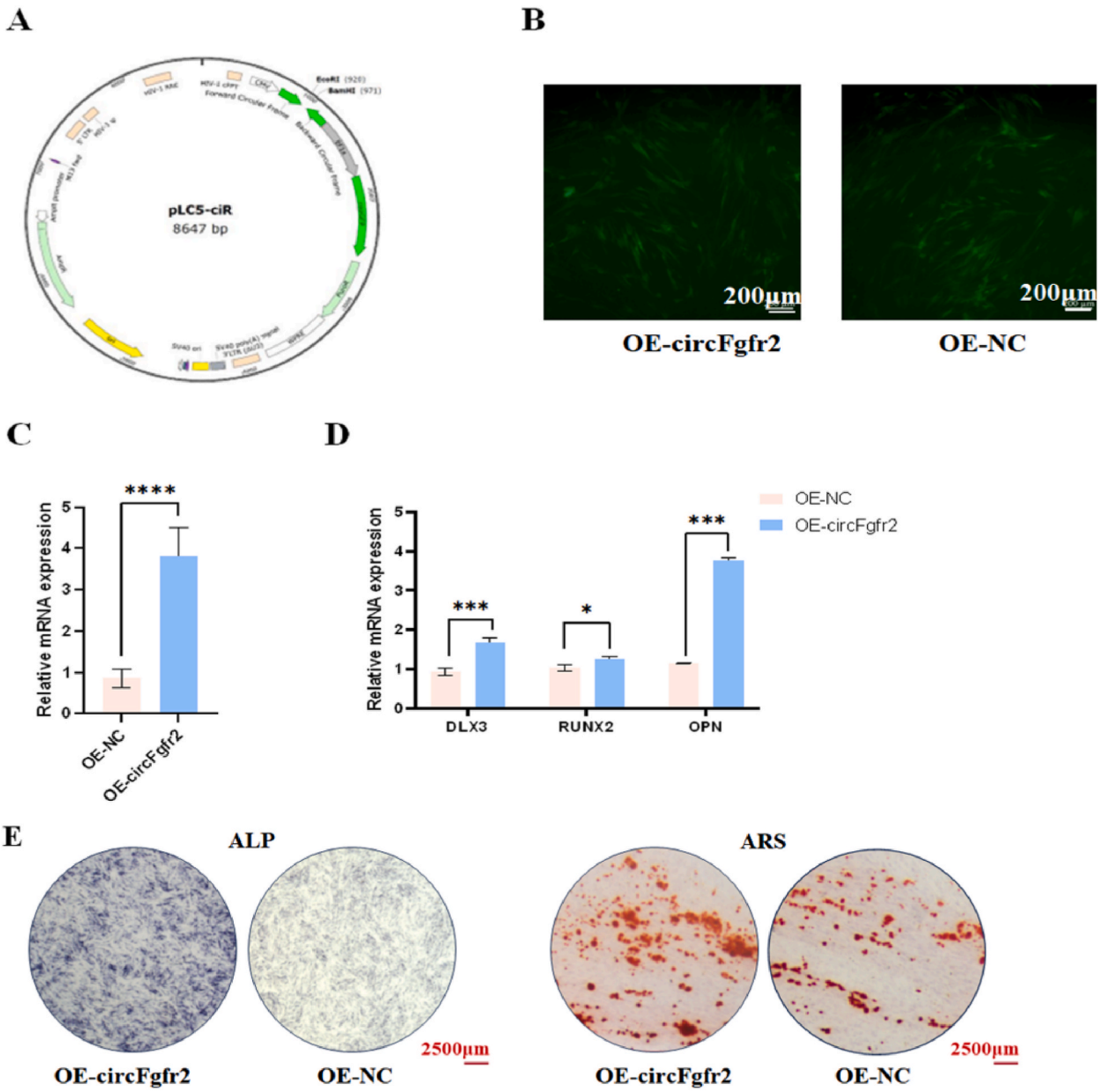

Fig. 3. CircFgfr2 promoted osteogenic differentiation of DFCs *in vitro* (A) Construction of the circFgfr2 overexpression vector. (B) Fluorescence to evaluate the efficiency of viral transfection for circFgfr2 overexpression. Scale bar: 200 μm (C) The mRNA expression levels of circFgfr2 in the OE-circFgfr2 and OE-NC groups. (D) The mRNA expression levels of DLX3, RUNX2, and OPN in the OE-circFgfr2 and OE-NC groups. (E) Representative ALP and ARS images in the OE-circFgfr2 and OE-NC groups. $^{*}P < 0.05$, $^{**}P < 0.01$, $^{***}P < 0.001$, and $^{****}P < 0.0001$.

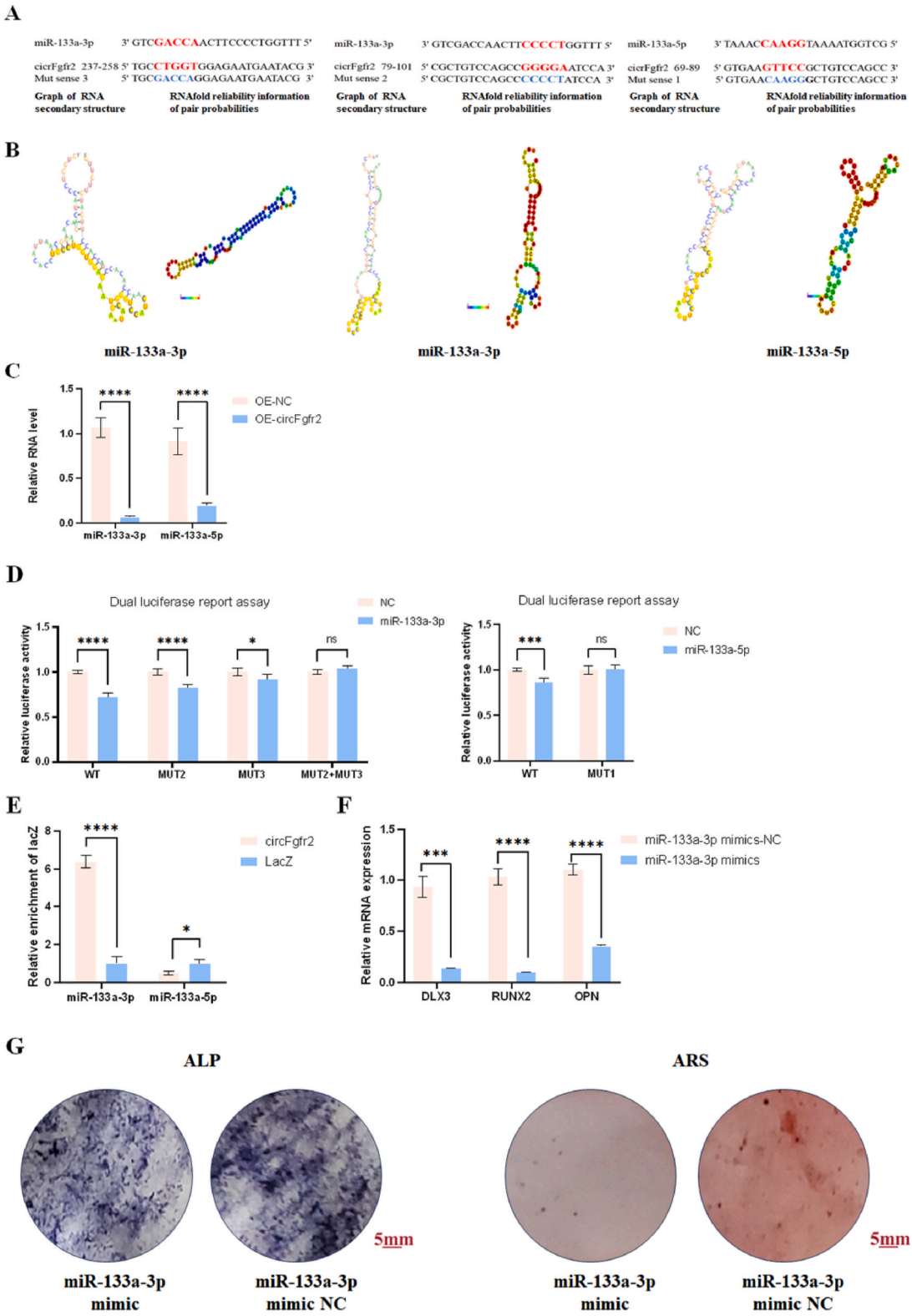

Fig. 4. CircFgfr2 acted as a sponge for miR-133a-3p *in vitro* (A) Bioinformatics analysis identified binding sites on miR-133a-3p for circFgfr2. (B) RegRNA predicted the potential interaction models between miR-133a-3p, miR-133a-5p, and circFgfr2. (C) The mRNA expression of miR-133a-3p and miR-133a-5p after transfection with the OE-circFgfr2 in DFCs. (D) Dual-luciferase reporter assay showed that both miR-133a-3p and miR-133a-5p effectively inhibited the luciferase activity of circFgfr2. (E) ChIRP analysis revealed that only miR-133a-3p was significantly enriched in the

pellet pulled down by the circFgfr2 probes. (F) The mRNA expression levels of DLX3, RUNX2, and OPN in the miR-133a-3p mimic and miR-133a-3p mimic NC groups. (G) Representative ALP and ARS images of the miR-133a-3p mimic and miR-133a-3p mimic NC groups. *$P < 0.05$, **$P < 0.01$, ***$P < 0.001$, and ****$P < 0.0001$.

3. Results

3.1. Workflow

The workflow of this study is depicted in Fig. 1.

3.2. Characterization of DFCs and circFgfr2

The DFCs displayed a polygonal or elongated spindle morphology (Fig. 2A). FCM was used to confirm stem cell properties (Fig. 2B). The analysis revealed that DFCs expressed positive markers for mesenchymal stem cells (MSCs), namely CD29, CD90, and CD44, but were negative for CD34 and CD45 (Fig. 2B). Sanger sequencing showed that circFgfr2 originated from the Fgfr2 gene exons 5 and 6 and was located on chr1: 200648164–200658087, with a length of 9630 bp (Fig. 2C). Agarose gel electrophoresis confirmed the resistance to RNase R digestion (Fig. 2D). Moreover, fluorescence *in situ* hybridization examination demonstrated that circFgfr2 was primarily localized in the cytoplasm of DFCs (Fig. 2E).

3.3. CircFgfr2 promoted osteogenic differentiation of DFCs in vitro

To thoroughly explore the impact of circFgfr2 on DFC differentiation, we constructed a circFgfr2 overexpression vector (pLC5-ciR-circFgfr2) and transfected it into DFCs (Fig. 3A and B). Compared to the control group, the overexpression group exhibited significantly higher levels of circFgfr2 (Fig. 3B and C). To investigate the role of circFgfr2, we detected osteogenic markers, including DLX3, RUNX2, and OPN. The results showed that circFgfr2 significantly increased the mRNA levels of DLX3, RUNX2, and OPN compared to those in the control group (Fig. 3d). ALP staining intensity was stronger in the overexpression (OE)-circFgfr2 group than in the negative control (NC) group (Fig. 3E). Similarly, more calcified nodules were observed in the OE-circFgfr2 group than in the NC group (Fig. 3E). The ALP activity and ARS quantity were higher in the OE-circFgfr2 group than in the OE-NC group (Fig. 3E).

3.4. CircFgfr2 acted as a sponge for miR-133a-3p in vitro

In a previous study, we hypothesized that circFgfr2 functions as an miRNA sponge [13]. RegRNA 2.0 was used to predict potential

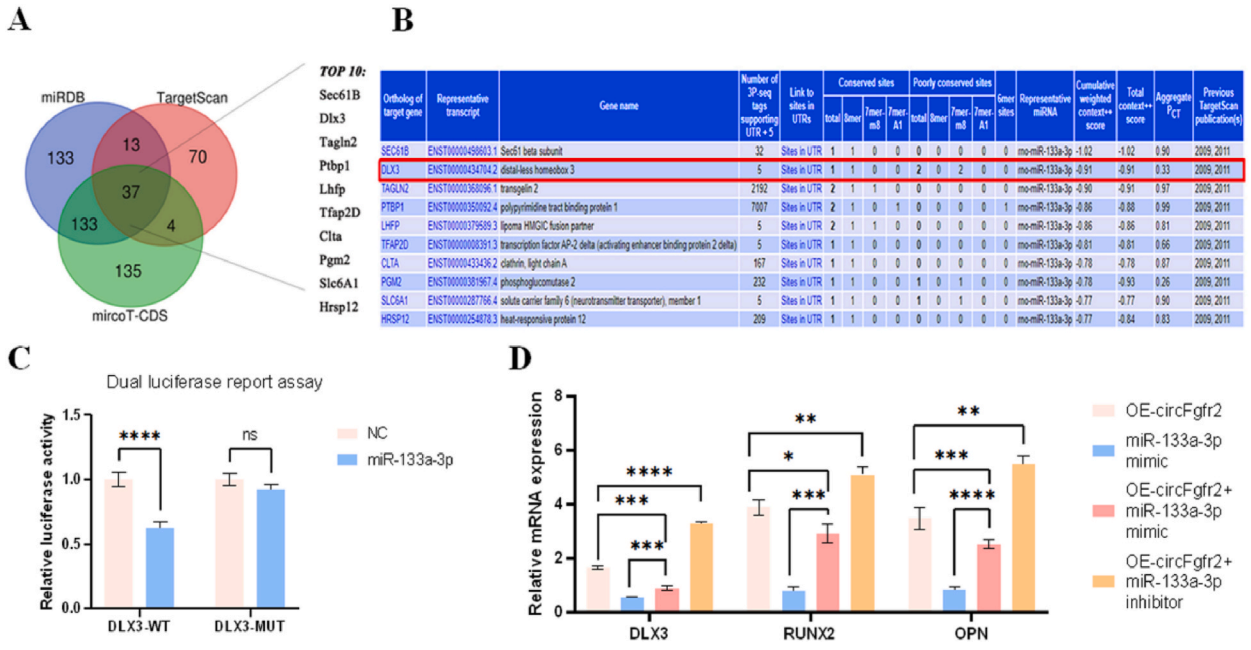

Ortholog of target gene	Representative transcript	Gene name	Number of 3P-seq tags supporting UTR+5	Link to sites in UTRs	Conserved sites				Poorly conserved sites				6mer sites	Representative miRNA	Cumulative weighted context++ score	Total context++ score	Aggregate P_{CT}	Previous TargetScan publication(s)
					total	8mer	7mer-m8	7mer-A1	total	8mer	7mer-m8	7mer-A1						
SEC61B	ENST00000498603.1	Sec61 beta subunit	32	Sites in UTR	1	1	0	0	0	0	0	0	0	mo-miR-133a-3p	-1.02	-1.02	0.90	2009, 2011
DLX3	ENST00000434784.2	distal-less homeobox 3	5	Sites in UTR	1	1	0	0	2	0	2	0	0	mo-miR-133a-3p	-0.91	-0.91	0.33	2009, 2011
TAGLN2	ENST00000368096.1	transgelin 2	2192	Sites in UTR	2	1	1	0	0	0	0	0	0	mo-miR-133a-3p	-0.90	-0.91	0.97	2009, 2011
PTBP1	ENST00000350092.4	polypyrimidine tract binding protein 1	7007	Sites in UTR	2	1	0	1	0	0	0	0	1	mo-miR-133a-3p	-0.86	-0.88	0.99	2009, 2011
LHFP	ENST00000379589.3	lipoma HMGIC fusion partner	5	Sites in UTR	2	1	1	0	0	0	0	0	0	mo-miR-133a-3p	-0.86	-0.86	0.81	2009, 2011
TFAP2D	ENST00000008391.3	transcription factor AP-2 delta (activating enhancer binding protein 2 delta)	5	Sites in UTR	1	1	0	0	0	0	0	0	0	mo-miR-133a-3p	-0.81	-0.81	0.66	2009, 2011
CLTA	ENST00000433436.2	clathrin, light chain A	167	Sites in UTR	1	1	0	0	0	0	0	0	0	mo-miR-133a-3p	-0.78	-0.78	0.87	2009, 2011
PGM2	ENST00000381967.4	phosphoglucomutase 2	232	Sites in UTR	1	1	0	0	1	0	1	0	0	mo-miR-133a-3p	-0.78	-0.93	0.26	2009, 2011
SLC6A1	ENST00000287766.4	solute carrier family 6 (neurotransmitter transporter), member 1	5	Sites in UTR	1	1	0	0	1	0	1	0	0	mo-miR-133a-3p	-0.77	-0.77	0.90	2009, 2011
HRSP12	ENST00000254878.3	heat-responsive protein 12	209	Sites in UTR	1	1	0	0	0	0	0	0	0	mo-miR-133a-3p	-0.77	-0.84	0.83	2009, 2011

Fig. 5. CircFgfr2 promoted osteogenic differentiation of DFCs through the miR-133a-3p/DLX3 axis (A, B) Potential target genes of miR-133a-3p were predicted using bioinformatics software. (C) Relative luciferase activity of wild-type (WT) or mutant (MUT) DLX3 and miR-133a-3p mimics or NC co-transfection. (D) mRNA expression of DLX3, RUNX2, and OPN in the OE-circFgfr2, miR-133a-3p mimic, OE-circFgfr2+miR-133a-3p mimic, and OE-circFgfr2+miR-133a-3p inhibitor groups. *$P < 0.05$, **$P < 0.01$, ***$P < 0.001$, and ****$P < 0.0001$.

target miRNAs and their binding sites. MiR-133a was one of the most probable targets, in accordance with our previous study [13]. Bioinformatic analysis revealed two binding sites for miR-133a-3p and one binding site for miR-133a-5p on circFgfr2 (Fig. 4A). Potential interactions between miR-133a-3p, miR-133a-5p, and circFgfr2 were simulated using RegRNA (Fig. 4B). Overexpression of circFgfr2 significantly reduced the relative expression levels of both miR-133a-3p and miR-133a-5p (Fig. 4C). Dual-luciferase reporter assays confirmed that both miR-133a-3p and miR-133a-5p effectively inhibited the luciferase activity of the wild-type (WT) circIRF2 reporter gene but not that of the mutant (MUT) circIRF2 vector (Fig. 4D). Furthermore, chromatin isolation by RNA purification (ChIRP) analysis revealed significant enrichment of miR-133a-3p, but not miR-133a-5p, in the pellet pulled down by circFgfr2 probes compared to the control probes (Fig. 4E). The mRNA levels of DLX3, RUNX2, and OPN in the miR-133a-3p mimic group were significantly lower than those in the control group (Fig. 4F). The intensity of ALP staining was weaker in the miR-133a-3p group than in the NC group (Fig. 4G). Fewer calcified nodules were observed in the miR-133a-3p group than in the NC group (Fig. 4G). Collectively, these findings strongly indicated that circFgfr2 functions as a sponge for miR-133a-3p.

3.5. *CircFgfr2 promoted osteogenic differentiation of DFCs through the miR-133a-3p/DLX3 axis*

Because miRNAs primarily function by directly targeting mRNAs, potential downstream targets of miR-133a-3p were predicted using the miRDB, microT-CDS, and TargetScan databases (Fig. 5A). Among the top ten predicted downstream targets of miR-133a-3p, DLX3 was identified and reported to be involved in osteogenesis (Fig. 5B). Dual-luciferase reporter assays were performed to investigate the direct interactions between miR-133a-3p and DLX3. The results indicated that miR-133a-3p overexpression significantly reduced the activity of the luciferase reporter containing WT DLX3. However, this effect was abolished when the binding sites for miR-133a-3p were mutated (Fig. 5C). Furthermore, the overexpression of miR-133a-3p significantly decreased DLX3 mRNA levels in DFCs compared to those in the control group (Fig. 4F). These findings strongly suggested that DLX3 is a direct target of miR-133a-3p. We co-transfected cells with miR-133a-3p mimics and inhibitors and performed rescue experiments. Regarding the mRNA levels of osteogenic markers, the results showed that miR-133a-3p mimics partially suppressed the increase in circFgfr2 expression, resulting in decreased DLX3, RUNX2, and OPN expression. Conversely, the miR-133a-3p inhibitor restored the downregulation of DLX3, RUNX2, and OPN (Fig. 5D). In conclusion, circFgfr2 promotes osteogenic differentiation of DFCs through the miR-133a-3p/DLX3 axis.

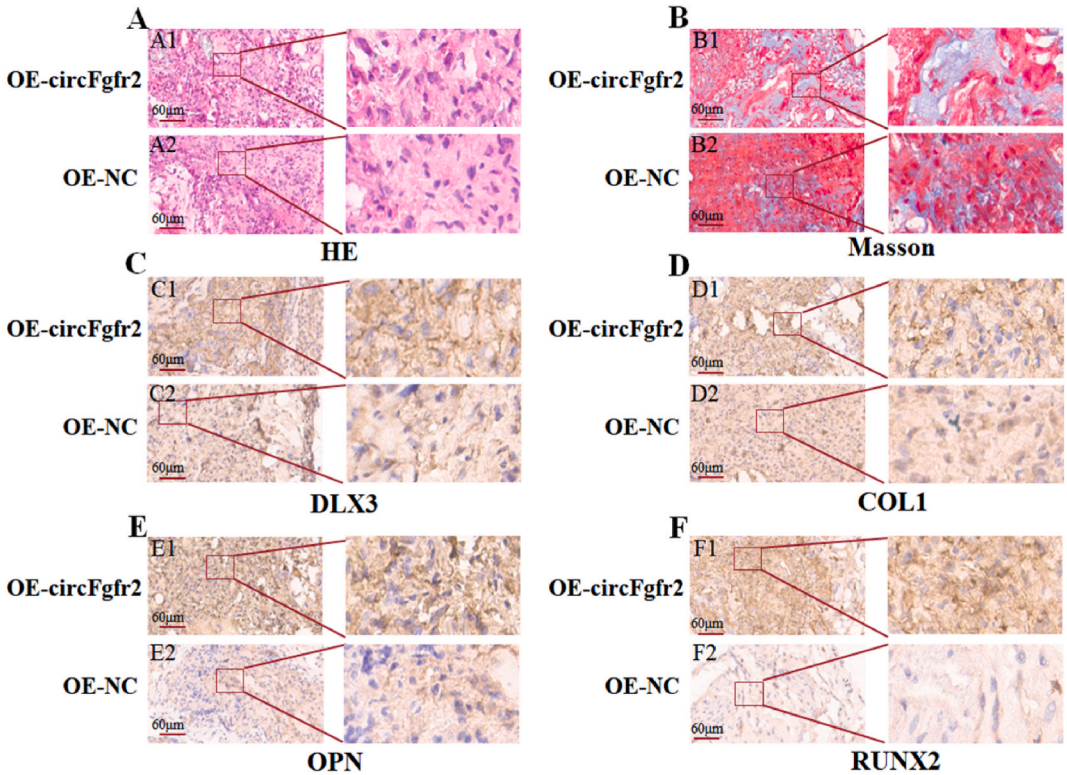

Fig. 6. CircFgfr2 enhances osteogenesis *in vivo* (A) H&E staining and (B) Masson's trichrome staining of the composites ($DFC^{OE\text{-}circFgfr2}$/β-TCP and $DFC^{NC\text{-}circFgfr2}$/β-TCP scaffolds) after subcutaneous transplantation in immunodeficient mice for 8 weeks. (C) Anti-DLX3, (D) Anti-COL1, (E) Anti-OPN and (F) Anti-RUNX2 immunohistochemistry staining of the composites. Scale bar: 60 μm.

3.6. CircFgfr2 enhanced osteogenesis in vivo

To further investigate the role of circFgfr2 in osteogenesis *in vivo*, β-TCP scaffolds were implanted in the subcutaneous tissue of mice with DFCs, and histological analyses were carried out. HE staining showed that circFgfr2 overexpression markedly enhanced new bone-like tissue formation with upregulated bone mineral areas (Fig. 6A). Masson's trichrome staining showed that circFgfr2 overexpression increased the new bone volume in the scaffold tissue compared to that in the control groups (Fig. 6B). Immunohistochemistry was performed for DLX3, COL1, OPN, and RUNX2 in the surrounding bone tissue, which exhibited brown staining. The areas for DLX3, COL1, OPN, and RUNX2 in the OE-circFgfr2 groups were larger than those in the control group (Fig. 6C–F).

4. Discussion

Over the past decade, researchers have shown that circRNAs play critical roles in tissue development [20–24], yet their specific roles in tooth development remain unclear. Our previous study showed that circFgfr2 expression increased while miR-133 expression decreased during osteogenic differentiation in DFCs. Moreover, we elucidated the role of circFgfr2 as a facilitator during osteogenesis, potentially serving as a sponge for miR-133; however, we could not elucidate the underlying mechanism [13]. Consequently, this study was designed to further investigate the function of circFgfr2 during osteogenic differentiation and identify the circRNA-miRNA-gene pathway.

First, we analyzed the characterization of circFgfr2, including genomic locus, back-splice junction site, closed-loop structure, and subcellular localization. We demonstrated that circFgfr2 is primarily localized in the cytoplasm of DFCs. In this study, we evaluated the role of circFgfr2 in osteogenesis. Our data indicated that circFgfr2 significantly increased the expression of the osteogenic markers RUNX2, OPN, and DLX3 compared with the control group. CircRNAs have a variety of functional mechanisms in cells: serving as miRNA sponges, interacting with proteins, regulating gene splicing or transcription, facilitating protein or peptide translation, and participating in epigenetic regulation [25,26]. Overexpression of circFgfr2 accelerates myogenic differentiation and myotube formation, thereby counteracting the inhibitory effects of miR-133a-5p and miR-29b-1-5p on chicken myoblasts [27]. The cytoplasmic localization of circFgfr2 suggests that it may act as an miRNA sponge.

We then investigated circRNA–miRNA interactions. Consistent with our previous study, we found that miR-133a-3p and miR-133a-5p are potential target miRNAs of circFgfr2. The binding sites for miR-133a-3p and miR-133a-5p on circFgfr2 were predicted using bioinformatics analysis. Our study confirmed that mir-133a-3p is regulated by circFgfr2 by sponging it. Next, we investigated the regulatory role of miR-133a-3p in the osteogenic differentiation of DFCs. Numerous studies have elucidated the functions of miRNAs in osteogenesis. MiRNAs regulate gene expression by either inhibiting mRNA translation or promoting mRNA degradation by binding to the 3′-untranslated region of target genes [28]. Previous studies have shown that miRNAs can regulate osteogenic differentiation positively or negatively [29–31]. MiRNAs target multiple genes by inducing translational repression and mRNA degradation. DLX3 is a target of miR-133a-3p and plays a significant role in osteogenic differentiation. DLX3 mRNA is expressed at relatively high levels in osteoblasts and stimulates osteoblastic differentiation [32]. DLX3 also influences cell proliferation and enhances the osteogenic differentiation of iPSC-MSCs [33]. Deletion of DLX3 in neural crest cells is associated with decreased bone formation and mineralization in craniofacial bones [34]. One study found that the transfection of miR-133a mimics in C2C12 premyoblast cells resulted in decreased DLX3 protein expression [35]. Consistent with this, we found that miR-133a-3p inhibited DLX3 expression, which was attenuated by circFgfr2 overexpression. However, further research is required to fully understand how DLX3 affects DFC differentiation.

It has been reported that DLX3 regulates the transcription of RUNX2 by binding to its promoters during osteogenic differentiation [36]. RUNX2, a BMP response gene, is essential for early bone formation [37]. RNA and chromatin immunoprecipitation sequencing analyses revealed that DLX3 regulates RUNX2 [38], while small-interfering RNA knockdown studies in osteoblasts have validated DLX3 as a potent regulator of RUNX2 [36]. RUNX2 was identified as a direct target of miR-133a by a co-transfection experiment in vascular smooth muscle cells with luciferase reporter plasmids containing WT or mutated 3′-untranslated region sequences of RUNX2. It has also been reported that the overexpression of miR-133a suppresses osteogenic differentiation of vascular smooth muscle cells, resulting in decreased RUNX2 expression [39]. A decrease in RUNX2 protein accumulation was observed following transfection with miR-133a in osteoblasts and chondrocytes [40]. Moreover, inhibition of miR-133a expression using ibandronate enhanced RUNX2 mRNA expression in PDLSCs [41]. In this study, miR-133a-3p was found to suppress osteogenic differentiation, as well as DLX3 and RUNX2 expression, in DFCs. Given that RUNX2 is a downstream target of DLX3, these findings suggest that miR-133a-3p directly and indirectly inhibits osteogenesis by targeting RUNX2 and DLX3. However, it is essential that future studies investigate how DLX3 regulates RUNX2 expression.

At the forefront of next-generation RNA therapeutics, circRNAs are anticipated to treat a diverse range of diseases. In contrast to the constrained applications of linear mRNA vaccines, which suffer from instability, inefficiency, and innate immunogenicity, circRNA vaccines, incorporating internal ribosome entry sites and open reading frames, present an enhanced approach to RNA-based vaccination. This method ensures safety, stability, ease of manufacturing, and scalability [42]. CircRNAs have been effectively utilized in several Sars-CoV-2 vaccines, resulting in the increased production of neutralizing antibodies. An illustration of this is the circRNA vaccine (VFLIP-X), employing an LNP delivery system, which generates a potent neutralizing antibody response against various Sars-CoV-2 mutants in mice through immunization with 5 μg of circRNA [43]. Furthermore, studies have revealed that circRNA vaccines effectively suppress tumor metastasis and demonstrate encouraging immune efficacy in mice [44]. In this study, we found that circFgfr2 enhances new bone formation and osteogenic gene expression *in vivo*. Overall, our findings provide a novel biomarker for bone diseases and a potential therapeutic target for bone regeneration.

In summary, this study demonstrates that circFgfr2 acts as a sponge for miR-133a-3p, thus positively regulating the osteogenic

differentiation of DFCs. The circFgfr2/miR-133a-3p/DLX3 axis is a novel therapeutic target for bone regeneration using DFCs.

Preprint

A previous version of this manuscript was published as a preprint [45].

Declarations

The authors declare that they have no known competing financial interests or personal relationships that could have appeared to influence the work reported in this paper.

Ethical Statement

The study was conducted in accordance with the National Institutes of Health guidelines on the ethical use of animals. All experiments were performed with the approval of the Ethics Committee of Sun Yat-sen University. The experimental animals were purchased from the Laboratory Animal Center of Sun Yat-sen University (License: SYSU-IACUC-2022-001346 and SYSU-IACUC-2022-B0004)

Funding

This work was supported by the Natural Science Foundation of Guangdong Province (No. 2021A1515010845) and Medical Scientific Research Foundation of Guangdong Province (No. A2022126).

Disclosure instructions

During the preparation of this work the author(s) used chatGPT in order to improve readability and language. After using this tool, authors reviewed and edited the content as needed and take full responsibility for the content of the publication.

Data availability statement

Data will be made available on request.

CRediT authorship contribution statement

Cheng Xu: Writing – original draft, Visualization, Validation, Methodology, Investigation, Conceptualization. **Zhiqing Xu:** Writing – original draft, Visualization, Validation, Methodology, Investigation. **Guixian Li:** Visualization, Validation, Methodology, Investigation. **Jing Li:** Validation, Methodology, Investigation. **Li Ye:** Validation, Investigation. **Yang Ning:** Writing – review & editing, Supervision, Funding acquisition. **Yu Du:** Writing – review & editing, Project administration, Funding acquisition, Conceptualization.

Declaration of competing interest

The authors declare that they have no known competing financial interests or personal relationships that could have appeared to influence the work reported in this paper.

Acknowledgements

We would like to express our gratitude to Hospital of Stomatology, Guangdong Provincial Key Laboratory of Stomatology, Guanghua School of Stomatology, Sun Yat-sen University for providing synthesis and characterization facilities.

References

[1] J. Slots, Periodontitis: facts, fallacies and the future, Periodontology 75 (2017) 7–23, 2000.
[2] T. Kwon, I.B. Lamster, L. Levin, Current concepts in the management of periodontitis, Int. Dent. J. 71 (2021) 462–476.
[3] S.L. Bee, Z.A.A. Hamid, Asymmetric resorbable-based dental barrier membrane for periodontal guided tissue regeneration and guided bone regeneration: a review, J. Biomed. Mater. Res. B Appl. Biomater. 110 (2022) 2157–2182.
[4] S. Guo, J. Kang, B. Ji, W. Guo, Y. Ding, Y. Wu, W. Tian, Periodontal-Derived mesenchymal cell sheets promote periodontal regeneration in inflammatory microenvironment, Tissue Eng. 23 (2017) 585–596.
[5] S. Qu, X. Yang, X. Li, J. Wang, Y. Gao, R. Shang, W. Sun, K. Dou, H. Li, Circular RNA: a new star of noncoding RNAs, Cancer Lett. 365 (2015) 141–148.
[6] J. Salzman, C. Gawad, P.L. Wang, N. Lacayo, P.O. Brown, Circular RNAs are the predominant transcript isoform from hundreds of human genes in diverse cell types, PLoS One 7 (2012) e30733.
[7] F. Ji, J. Pan, Z. Shen, Z. Yang, J. Wang, X. Bai, J. Tao, The circular RNA circRNA124534 promotes osteogenic differentiation of human dental pulp stem cells through modulation of the miR-496/beta-Catenin pathway, Front. Cell Dev. Biol. 8 (2020) 230.
[8] L.L. Chen, The biogenesis and emerging roles of circular RNAs, Nat. Rev. Mol. Cell Biol. 17 (2016) 205–211.

[9] H.L. Sanger, G. Klotz, D. Riesner, H.J. Gross, A.K. Kleinschmidt, Viroids are single-stranded covalently closed circular RNA molecules existing as highly base-paired rod-like structures, Proc. Natl. Acad. Sci. U. S. A. 73 (1976) 3852–3856.
[10] W. Chia, J. Liu, Y.G. Huang, C. Zhang, A circular RNA derived from DAB1 promotes cell proliferation and osteogenic differentiation of BMSCs via RBPJ/DAB1 axis, Cell Death Dis. 11 (2020) 372.
[11] X. Huang, X. Cen, B. Zhang, Y. Liao, G. Zhu, J. Liu, Z. Zhao, Prospect of circular RNA in osteogenesis: a novel orchestrator of signaling pathways, J. Cell. Physiol. 234 (2019) 21450–21459.
[12] Z. Liu, S. Li, S. Xu, A.B.D.X.K. Neby, J. Wen, X. Zeng, X. Shen, P. Xu, Hsa_Circ_0005044 promotes osteo/odontogenic differentiation of dental pulp stem cell via modulating miR-296-3p/FOSL1, DNA Cell Biol. 42 (2023) 14–26.
[13] Y. Du, J. Li, Y. Hou, C. Chen, W. Long, H. Jiang, Alteration of circular RNA expression in rat dental follicle cells during osteogenic differentiation, J. Cell. Biochem. 120 (2019) 13289–13301.
[14] N. Ma, C. Tie, B. Yu, W. Zhang, J. Wan, Circular RNAs regulate its parental genes transcription in the AD mouse model using two methods of library construction, Faseb. J. 34 (2020) 10342–10356.
[15] L. Szabo, R. Morey, N.J. Palpant, P.L. Wang, N. Afari, C. Jiang, M.M. Parast, C.E. Murry, L.C. Laurent, J. Salzman, Statistically based splicing detection reveals neural enrichment and tissue-specific induction of circular RNA during human fetal development, Genome Biol. 16 (2015) 126.
[16] X. Li, Y. Zheng, Y. Zheng, Y. Huang, Y. Zhang, L. Jia, W. Li, Circular RNA CDR1as regulates osteoblastic differentiation of periodontal ligament stem cells via the miR-7/GDF5/SMAD and p38 MAPK signaling pathway, Stem Cell Res. Ther. 9 (2018) 232.
[17] C. Liang, W. Li, Q. Huang, Q. Wen, CircFKBP5 suppresses apoptosis and inflammation and promotes osteogenic differentiation, Int. Dent. J. 73 (2023) 377–386.
[18] X. Chen, H. Ouyang, Z. Wang, B. Chen, Q. Nie, A novel circular RNA generated by FGFR2 gene promotes myoblast proliferation and differentiation by sponging miR-133a-5p and miR-29b-1-5p, Cells 7 (2018).
[19] C. Chu, J. Quinn, H.Y. Chang, Chromatin isolation by RNA purification (ChIRP), J. Vis. Exp. 61 (2012).
[20] X. Guo, W. Tan, C. Wang, The emerging roles of exosomal circRNAs in diseases, Clin. Transl. Oncol. 23 (2021) 1020–1033.
[21] M.T. Veno, T.B. Hansen, S.T. Veno, B.H. Clausen, M. Grebing, B. Finsen, I.E. Holm, J. Kjems, Spatio-temporal regulation of circular RNA expression during porcine embryonic brain development, Genome Biol. 16 (2015) 245.
[22] Y. Ling, Q. Zheng, L. Zhu, L. Xu, M. Sui, Y. Zhang, Y. Liu, F. Fang, M. Chu, Y. Ma, X. Zhang, Trend analysis of the role of circular RNA in goat skeletal muscle development, BMC Genom. 21 (2020) 220.
[23] A. Qi, W. Ru, H. Yang, Y. Yang, J. Tang, S. Yang, X. Lan, C. Lei, X. Sun, H. Chen, Circular RNA ACTA1 acts as a sponge for miR-199a-5p and miR-433 to regulate bovine myoblast development through the MAP3K11/MAP2K7/JNK pathway, J. Agric. Food Chem. 70 (2022) 3357–3373.
[24] R.M. Zhang, Y. Pan, C.X. Zou, Q. An, J.R. Cheng, P.J. Li, Z.H. Zheng, Y. Pan, W.Y. Feng, S.F. Yang, D.S. Shi, Y.M. Wei, Y.F. Deng, CircUBE2Q2 promotes differentiation of cattle muscle stem cells and is a potential regulatory molecule of skeletal muscle development, BMC Genom. 23 (2022) 267.
[25] H. Su, T. Tao, Z. Yang, X. Kang, X. Zhang, D. Kang, S. Wu, C. Li, Circular RNA cTFRC acts as the sponge of MicroRNA-107 to promote bladder carcinoma progression, Mol. Cancer 18 (2019) 27.
[26] R. Wang, S. Zhang, X. Chen, N. Li, J. Li, R. Jia, Y. Pan, H. Liang, EIF4A3-induced circular RNA MMP9 (circMMP9) acts as a sponge of miR-124 and promotes glioblastoma multiforme cell tumorigenesis, Mol. Cancer 17 (2018) 166.
[27] R. Chen, T. Jiang, S. Lei, Y. She, H. Shi, S. Zhou, J. Ou, Y. Liu, Expression of circular RNAs during C2C12 myoblast differentiation and prediction of coding potential based on the number of open reading frames and N6-methyladenosine motifs, Cell Cycle 17 (2018) 1832–1845.
[28] E. van Rooij, N. Liu, E.N. Olson, MicroRNAs flex their muscles, Trends Genet. 24 (2008) 159–166.
[29] C. Zhao, Y. Gu, Y. Wang, Q. Qin, T. Wang, M. Huang, H. Zhang, Y. Qu, J. Zhang, Z. Du, X.X. Jiang, L. Xu, miR-129-5p promotes osteogenic differentiation of BMSCs and bone regeneration via repressing Dkk3, Stem Cell. Int. 2021 (2021) 7435605.
[30] L. Hu, X. Xie, H. Xue, T. Wang, A.C. Panayi, Z. Lin, Y. Xiong, F. Cao, C. Yan, L. Chen, P. Cheng, K. Zha, Y. Sun, G. Liu, C. Yu, Y. Hu, R. Tao, W. Zhou, B. Mi, G. Liu, MiR-1224-5p modulates osteogenesis by coordinating osteoblast/osteoclast differentiation via the Rap1 signaling target ADCY2, Exp. Mol. Med. 54 (2022) 961–972.
[31] Y. Tang, Y. Sun, J. Zeng, B. Yuan, Y. Zhao, X. Geng, L. Jia, S. Zhou, X. Chen, Exosomal miR-140-5p inhibits osteogenesis by targeting IGF1R and regulating the mTOR pathway in ossification of the posterior longitudinal ligament, J. Nanobiotechnol. 20 (2022) 452.
[32] H. Li, I. Marijanovic, M.S. Kronenberg, I. Erceg, M.L. Stover, D. Velonis, M. Mina, J.G. Heinrich, S.E. Harris, W.B. Upholt, I. Kalajzic, A.C. Lichtler, Expression and function of Dlx genes in the osteoblast lineage, Dev. Biol. 316 (2008) 458–470.
[33] J. Li, Q. Lin, Y. Lin, R. Lai, W. Zhang, Effects of DLX3 on the osteogenic differentiation of induced pluripotent stem cell-derived mesenchymal stem cells, Mol. Med. Rep. 23 (2021).
[34] O. Duverger, J. Isaac, A. Zah, J. Hwang, A. Berdal, J.B. Lian, M.I. Morasso, In vivo impact of Dlx3 conditional inactivation in neural crest-derived craniofacial bones, J. Cell. Physiol. 228 (2013) 654–664.
[35] A.S. Qadir, J. Lee, Y.S. Lee, K.M. Woo, H.M. Ryoo, J.H. Baek, Distal-less homeobox 3, a negative regulator of myogenesis, is downregulated by microRNA-133, J. Cell. Biochem. 120 (2019) 2226–2235.
[36] M.Q. Hassan, R.S. Tare, S.H. Lee, M. Mandeville, M.I. Morasso, A. Javed, A.J. van Wijnen, J.L. Stein, G.S. Stein, J.B. Lian, BMP2 commitment to the osteogenic lineage involves activation of Runx2 by DLX3 and a homeodomain transcriptional network, J. Biol. Chem. 281 (2006) 40515–40526.
[37] Z. Li, M.Q. Hassan, S. Volinia, A.J. van Wijnen, J.L. Stein, C.M. Croce, J.B. Lian, G.S. Stein, A microRNA signature for a BMP2-induced osteoblast lineage commitment program, Proc. Natl. Acad. Sci. U. S. A. 105 (2008) 13906–13911.
[38] J. Isaac, J. Erthal, J. Gordon, O. Duverger, H.W. Sun, A.C. Lichtler, G.S. Stein, J.B. Lian, M.I. Morasso, DLX3 regulates bone mass by targeting genes supporting osteoblast differentiation and mineral homeostasis in vivo, Cell Death Differ. 21 (2014) 1365–1376.
[39] X.B. Liao, Z.Y. Zhang, K. Yuan, Y. Liu, X. Feng, R.R. Cui, Y.R. Hu, Z.S. Yuan, L. Gu, S.J. Li, D.A. Mao, Q. Lu, X.M. Zhou, V.A. de Jesus Perez, L.Q. Yuan, MiR-133a modulates osteogenic differentiation of vascular smooth muscle cells, Endocrinology 154 (2013) 3344–3352.
[40] Y. Zhang, R.L. Xie, C.M. Croce, J.L. Stein, J.B. Lian, A.J. van Wijnen, G.S. Stein, A program of microRNAs controls osteogenic lineage progression by targeting transcription factor Runx2, Proc. Natl. Acad. Sci. U. S. A. 108 (2011) 9863–9868.
[41] Q. Zhou, Z.N. Zhao, J.T. Cheng, B. Zhang, J. Xu, F. Huang, R.N. Zhao, Y.J. Chen, Ibandronate promotes osteogenic differentiation of periodontal ligament stem cells by regulating the expression of microRNAs, Biochem. Biophys. Res. Commun. 404 (2011) 127–132.
[42] D. Niu, Y. Wu, J. Lian, Circular RNA vaccine in disease prevention and treatment, Signal Transduct. Targeted Ther. 8 (2023) 341.
[43] C. Seephetdee, K. Bhukhai, N. Buasri, P. Leelukkanaveera, P. Lerdwattanasombat, S. Manopwisedjaroen, N. Phueakphud, S. Kuhaudomlarp, E. Olmedillas, E. O. Saphire, A. Thitithanyanont, S. Hongeng, P. Wongtrakoongate, A circular mRNA vaccine prototype producing VFLIP-X spike confers a broad neutralization of SARS-CoV-2 variants by mouse sera, Antivir. Res. 204 (2022) 105370.
[44] H. Li, K. Peng, K. Yang, W. Ma, S. Qi, X. Yu, J. He, X. Lin, G. Yu, Circular RNA cancer vaccines drive immunity in hard-to-treat malignancies, Theranostics 12 (2022) 6422–6436.
[45] Yu Du, Cheng Xu, Guixian Li, et al., Circular RNA CircFgfr2 promotes osteogenic differentiation of rat dental follicle cells via sponging MicroRNA miR-133a-3p and up-regulating distal-less homeobox DLX3. PREPRINT (Version 1), Research Square, 2022, https://doi.org/10.21203/rs.3.rs-1181994/v1.